PHYSICAL REVIEW D **72,** 054017 (2005)

Simulating W/Z + jets production at the CERN LHC

Frank Krauss,* Andreas Schälicke,† Steffen Schumann,‡ and Gerhard Soff§

Institute for Theoretical Physics, D-01062 Dresden, Germany

(Received 4 April 2005; revised manuscript received 19 August 2005; published 23 September 2005)

The merging procedure of tree-level matrix elements and the subsequent parton shower as implemented in the new event generator SHERPA will be validated for the example of single gauge boson production at the CERN LHC. The validation includes consistency checks and comparisons to results obtained from other event generators. In particular, comparisons with full next-to-leading order QCD calculations prove SHERPA's ability to correctly account for additional hard QCD radiation present in these processes.

DOI: 10.1103/PhysRevD.72.054017 PACS numbers: 13.85.−t, 13.85.Qk, 13.87.−a

I. INTRODUCTION

The production of electroweak gauge bosons, which decay leptonically, is one of the most prominent examples for hard processes at hadron colliders and one of the first applications of perturbative QCD in such reactions. In fact, the next-to-leading order (NLO) corrections to this process in QCD, calculated by [1–5], provided the first calculation of such corrections for hadron collisions. Later, their production cross section has been calculated at next-to-next-to-leading order (NNLO) by [6,7]. Recently, the first distribution determined at NNLO related to these processes, namely, the boson rapidity, has been calculated by [8]. In addition, there is a large number of computer programs dealing with single gauge boson production. They range from RESBOS [9], which resums soft gluon effects in these processes, to codes, that evaluate cross sections at the LO level for the production of gauge bosons accompanied by jets. Examples for the latter include specialized ones, such as VECBOS [10], and general ones, usually called parton level generators, such as COMPHEP [11], GRACE/GR@PPA [12,13], MADGRAPH/MADEVENT [14,15], ALPGEN [16], and AMEGIC++ [17]. Furthermore, the first package called MCFM has been made available that calculates total and differential cross sections at NLO precision for the production of gauge bosons with up to two jets [18,19]. This reflects the importance of this particular process. At the CERN LHC, starting to provide pp collisions at $\sqrt{s} =$ 15 TeV in the near future, the gauge bosons will be produced with unprecedented rates. For instance, at luminosities of $\mathcal{L} \approx 10^{33}$ cm^2/s the production and leptonic decay of a single W boson will occur with a frequency of around 20 Hz, rendering this process a prime candidate for luminosity monitoring [20–23]. Of course, these large rates will allow one to measure the gauge bosons' parameters, such as their masses and widths, with a precision [24,25] beyond what could be reached at previous collider experiments [26–35]. At the CERN LHC, the production of W and Z bosons together with jets also constitutes an important background to all kinds of searches for new physics, such as supersymmetry. An example of this is the production and decay of gluinos, where the production of jets plus a Z boson decaying into neutrinos forms a major background.

In a previous analysis [36] it has been shown that some results for this type of process, i.e. the production of single gauge bosons plus extra jets, as obtained by other multipurpose event generators such as PYTHIA [37,38], HERWIG [39,40], or even MC@NLO [41–43], differ significantly from the results obtained by SHERPA [44]. In particular, it has been shown already that at the Fermilab Tevatron, operating at roughly 2 TeV center-of-mass energy, the additional jets are produced at significantly larger transverse momenta. The reason for this difference is the way the different codes implement the knowledge of exact matrix elements for the production of multiparticle final states. In both, PYTHIA and HERWIG, they are included at first order in α_S through a correction of the first hard emission on the corresponding $q\bar{q} \to Vg$ or $qg \to Vq$ matrix element, where V stands for the vector boson [45–47]. In MC@NLO, the full first order correction, including both the virtual and the real parts, is matched with the parton shower. This has the additional benefit that MC@NLO reproduces correctly the total production rate of single gauge bosons and the spectrum of the first additional jet at first order in α_S. In contrast, in SHERPA a method has been implemented that consistently adds different matrix elements at the tree level for different jet multiplicities and merges them with the parton shower. The basic idea in this approach is to internally define a region of jet production (hard parton emissions) and a region of jet evolution (soft parton emissions). The two regimes are divided by a $k_\perp$ type of jet measure [48–50]. Leading higher order effects are incorporated by reweighting the matrix elements with appropriate Sudakov form factors. Formal independence at leading logarithmic order of the overall result on the jet measure is achieved by suitable starting conditions and vetoing hard emissions inside the parton shower. This approach was presented for the first time [51] for e^+e^- collisions; it has been extended to hadronic collisions in

*Electronic address: krauss@theory.phy.tu-dresden.de
†Electronic address: dreas@theory.phy.tu-dresden.de
‡Electronic address: steffen@theory.phy.tu-dresden.de
§Deceased

[52]. A reformulation for dipole cascades has been presented in [53]. The algorithm is implemented in a fully automated way, and in full generality in SHERPA, some other realizations [54,55] proved the flexibility and the validity of the approach.

In this publication, the previous analysis [36] will be extended to the case of the CERN LHC, operating in the pp mode at 14 TeV center-of-mass energy. In Sec. II, a number of consistency checks will focus on the independence of the results on variations of the internal jet definition and of the number of matrix elements involved. Also, the effect of scale variations in both the matrix elements and the parton shower is investigated there. Then, in Sec. III, results obtained with SHERPA will be contrasted to those obtained from fixed order (LO and NLO) calculations provided by MCFM. Following this, different multipurpose event generators, namely PYTHIA, MC@NLO, and SHERPA, will be compared in Sec. IV, before the findings will be summarized in the conclusions.

II. CONSISTENCY CHECKS

Before comparing the results of SHERPA with those of other programs, some consistency checks will be performed. To do so, the dependence of some observables in reactions of the type $pp \to e^+e^- + X$ on internal parameters intrinsic for the merging procedure will be investigated. In particular, these parameters are the internal jet resolution cut Q_{cut} and the maximal number n_{max} of final state partons (giving rise to jets) described through matrix elements. The former parameter defines the transition of the matrix element domain to the phase-space region covered by the parton shower during event generation. In principle, the actual value of this parameter can be chosen freely; nevertheless their exist criteria that guide such a choice. For very low values of Q_{cut} the evaluation of the matrix elements becomes very challenging and potentially inefficient once jet cuts are performed on the analysis level harder than the generation cut Q_{cut}. The upper limit is defined by the scale where jets produced by the parton shower start to disagree significantly from such produced by equivalent matrix elements. To study, especially, the effect of the upper limit, the values used in this analysis will range over nearly 1 order of magnitude, from 15 to 100 GeV. The choice of the number of matrix element partons taken into account may be steered by two aspects. First of all, n_{max} has to be sufficiently large to properly account for the phase-space region the observable under consideration is sensitive to. As an example, consider the transverse momentum of the boson compared to that of, say, the third jet. It is obvious that a rather inclusive quantity such as the former may be appropriately described with lower values of n_{max} than the latter observable. On the other hand, the upper limit on n_{max} is given by the availability of the matrix elements at all and by the potentially large amount of CPU time the evaluation of multileg matrix elements requires. Within SHERPA, matrix elements with up to four extra partons can be delivered for the processes under consideration in this publication. After evaluating the sensitivity of the results on the principal parameters defining the merging procedure, Q_{cut} and n_{max}, the effect of scale variations will be investigated. This, together with the dependence on Q_{cut} and n_{max}, yields an estimate for the uncertainty related to predictions of SHERPA.

The results presented in this section were generated with the following setups: when varying the jet resolution parameter Q_{cut}, the maximal number of final state partons n_{max} has been set to $n_{\mathrm{max}} = 3$. When studying the impact of different matrix element multiplicities, the scale Q_{cut} has been fixed to $Q_{\mathrm{cut}} = 15$ GeV; this clearly maximizes the impact of the higher order matrix elements. When scale variations are under consideration, the choices $Q_{\mathrm{cut}} = 20$ GeV and $n_{\mathrm{max}} = 2$ have been made.

In the following, Z-boson production will be investigated in more detail. Nevertheless, the process under consideration is $pp \to Z/\gamma^* \to e^+e^- + X$, where the full γ-Z interference is taken into account and spin correlations are fully respected. Further input parameters used and the phase-space cuts applied are summarized in Appendix A. Note that the cut on the invariant mass of the lepton pair is just $m_{ee} > 15$ GeV which is rather small. The description of such low mass lepton pairs constitutes a real challenge for the description through the merging prescription. The reason is that at large $Q_{\mathrm{cut}} = \mathcal{O}(100\ \mathrm{GeV})$, lepton pairs with such low invariant mass clearly are softer than any jet produced through the matrix element, rendering consistent merging a complicated task.

A. Observables related to the leptons

Starting from more inclusive observables, first of all, the effect of parameter variation on lepton observables will be considered. In Fig. 1, the $p_\perp$ spectra of both the lepton pair (upper row) and of the electron alone (lower row) are shown for three different values of Q_{cut}: from left to right, in the columns $Q_{\mathrm{cut}} = 15, 50, 100$ GeV, as indicated by the thin vertical lines. In each plot, the resulting spectrum is compared to a reference obtained from averaging the results for $Q_{\mathrm{cut}} = 15, 20, 30, 50, 100$ GeV. In this and all other plots, contributions stemming from the different matrix element multiplicities are indicated through additional lines.

Using $Q_{\mathrm{cut}} = 15$ GeV obviously produces the hardest boson/lepton spectrum. It is the smallest cut considered here and therefore the distributions are dominated by matrix elements that, in contrast to the parton shower, favor rather hard parton kinematics. For very high $p_\perp$ the distributions are almost completely covered by the matrix element with the highest multiplicity ($n_{\mathrm{max}} = 3$). This shows that the LHC provides enough phase space to produce a sufficient amount of events with three and more jets

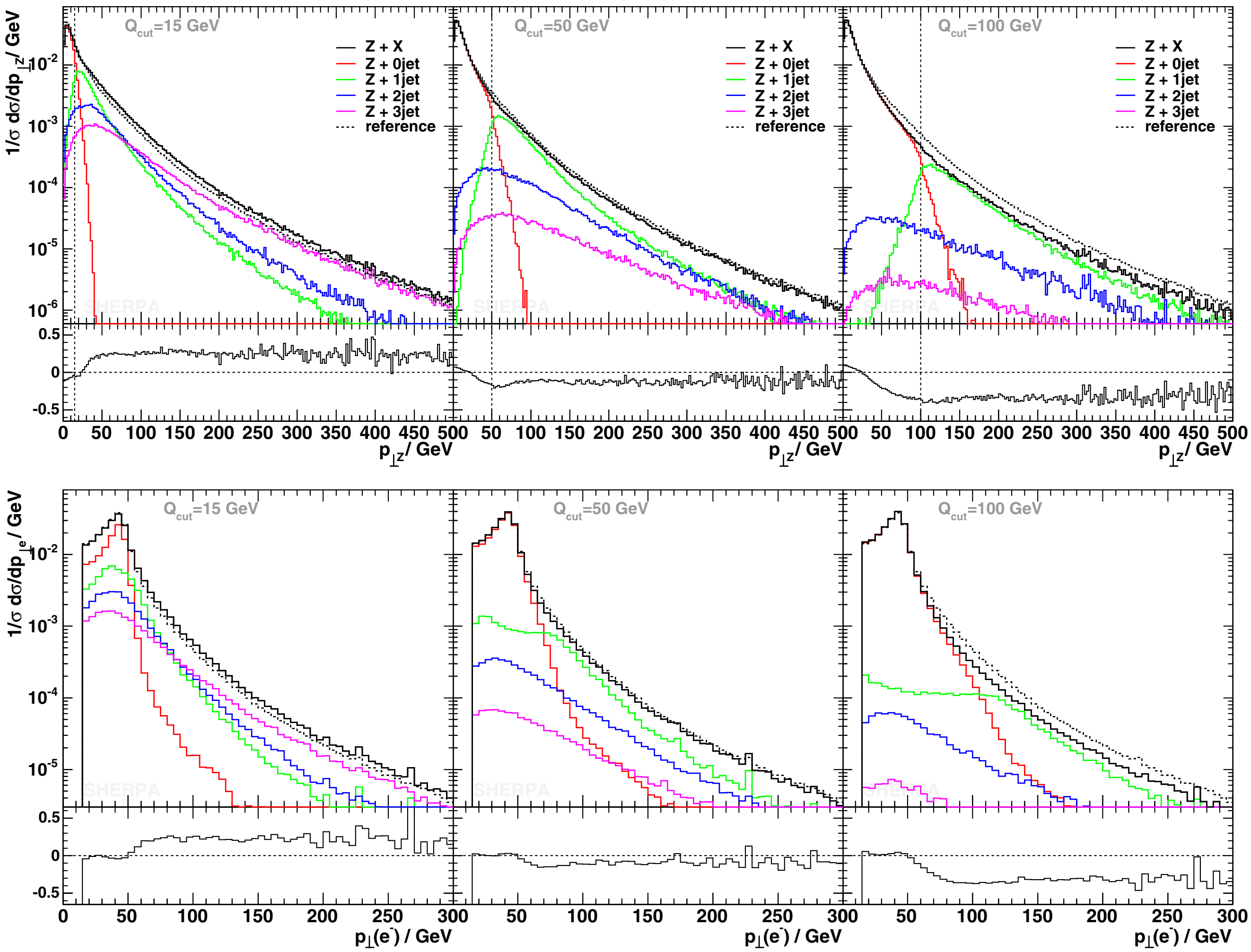

FIG. 1 (color online). $p_\perp(Z)$ (upper row) and $p_\perp(e^-)$ (lower row) for $Q_{\rm cut} = 15$ GeV, 50 GeV, and 100 GeV (from left to right). The dashed reference spectrum has been obtained after averaging the results for $Q_{\rm cut} = 15, 20, 30, 50, 100$ GeV. In the lower part of each plot the variations of the result with respect to the corresponding reference curve are presented.

of $p_\perp > Q_{\rm cut}$. For the case of $Q_{\rm cut} = 50$ GeV the situation is slightly different. The high-$p_\perp$ tail is filled to an equal amount by the different multiplicities, the total sum being slightly below the reference curve. This reference curve contains three results with jet resolutions smaller than 50 GeV that somehow dominate the averaged result. With respect to (w.r.t.) the reference, the spectrum for $Q_{\rm cut} = 100$ GeV starts to underestimate the boson transverse momentum at $p_\perp \approx 35$ GeV and the lepton $p_\perp$ for values larger than 60 GeV. To understand this, one has to remember that the boson transverse momentum for values below the resolution cut is almost completely covered by the parton shower. The shower description, however, is known to suffer from a lack of hard QCD radiation. This does not leave enough hard partons that the boson can recoil against. Beyond this influence of the $Q_{\rm cut}$ variation on the intermediate and high boson transverse momenta, it has to be noted that all curves are very smooth around the jet resolution cut. Although the cut defines a rather sharp transition from the parton shower to the matrix element domain, no significant holes in the boson and lepton $p_\perp$ spectra can be observed.

In Fig. 2 the pseudorapidity spectra of the lepton pair and the single electron are displayed, again for $Q_{\rm cut} = 15$, 50, 100 GeV with the same way of generating the reference. While the electron observable is nearly unaltered, the differences in the η distribution of the lepton pair can be understood easily: the smaller the chosen cut, the larger the influence of the matrix elements with extra external legs. Since matrix elements cover the region of phase space where large angle hard emissions are important, they prefer to give the boson much more transverse momentum and therefore produce them much more central in pseudorapidity than the parton shower does. This effect yields slightly tighter spectra with the central rapidities being pronounced for smaller resolution cuts.

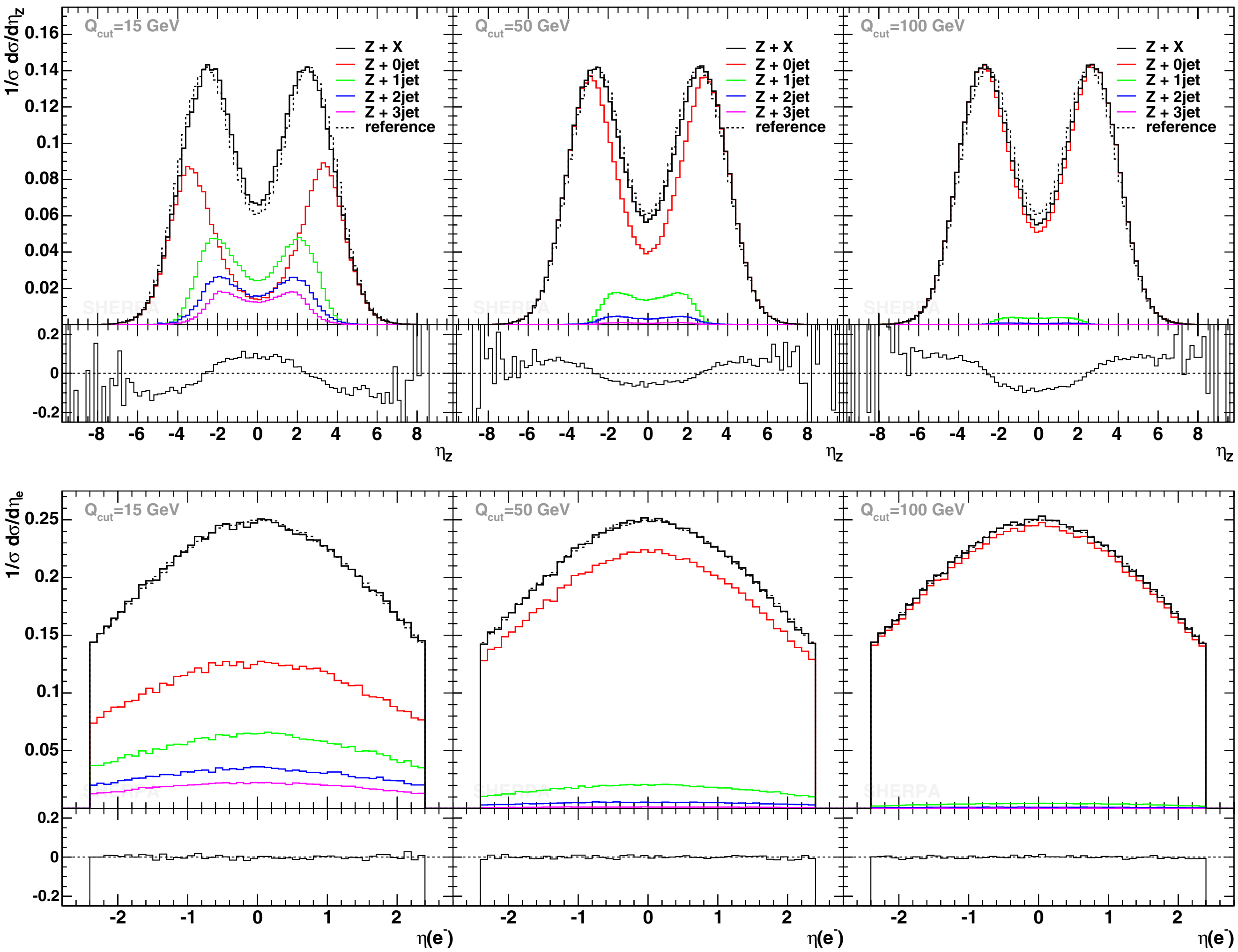

FIG. 2 (color online). $\eta(Z)$ (upper row) and $\eta(e^-)$ (lower row) for $Q_{\rm cut} = 15$ GeV, 50 GeV, and 100 GeV (from left to right). The dashed reference spectrum has been obtained after averaging the results for $Q_{\rm cut} = 15, 20, 30, 50, 100$ GeV. In the lower part of each plot the variations of the result with respect to the corresponding reference curve are presented.

The effect of varying $n_{\rm max}$ on the transverse momentum and pseudorapidity spectrum of the lepton pair is exhibited in Fig. 3. In this figure, results are compared for $n_{\rm max} = 2, 3, 4$. In each plot, a reference result is given with the corresponding $n_{\rm max}^{\rm ref} = n_{\rm max} - 1$. For the case of the $p_\perp$ distribution it has already been observed that the high-$p_\perp$ region is described through higher multiplicity matrix elements. As a consequence, it is the high-$p_\perp$ region that is affected by the variation of $n_{\rm max}$. However, while the effect is clearly noticeable when going from one to two extra partons, the change becomes smaller the more matrix elements are included. From the very right plot one can conclude that considering $Z + 3$ extra parton matrix elements is a reasonable choice to simulate inclusive Z production. The change in the η distribution for different $n_{\rm max}$ is as expected, considering what has already been seen for varying the jet resolution. The higher multiplicity matrix elements favor the region of small $|\eta|$ yielding slightly tighter pseudorapidity distributions. Again, the more matrix elements have been taken into account the smaller the influence when adding an even higher multiplicity.

In comparison to what has been observed when studying gauge boson production at the Fermilab Tevatron [36], the LHC provides much more phase space for additional hard QCD radiation, enhancing the influence of higher order matrix elements. Therefore a modest value of the jet resolution parameter and the inclusion of a sufficient large number of matrix element legs is advisable for LHC analyses.

B. Jet observables

As has already been seen in the previous publication [36], a very sensitive test of the merging procedure is provided by observables based on jets. In particular, differential jet rates have turned out to be very useful, since

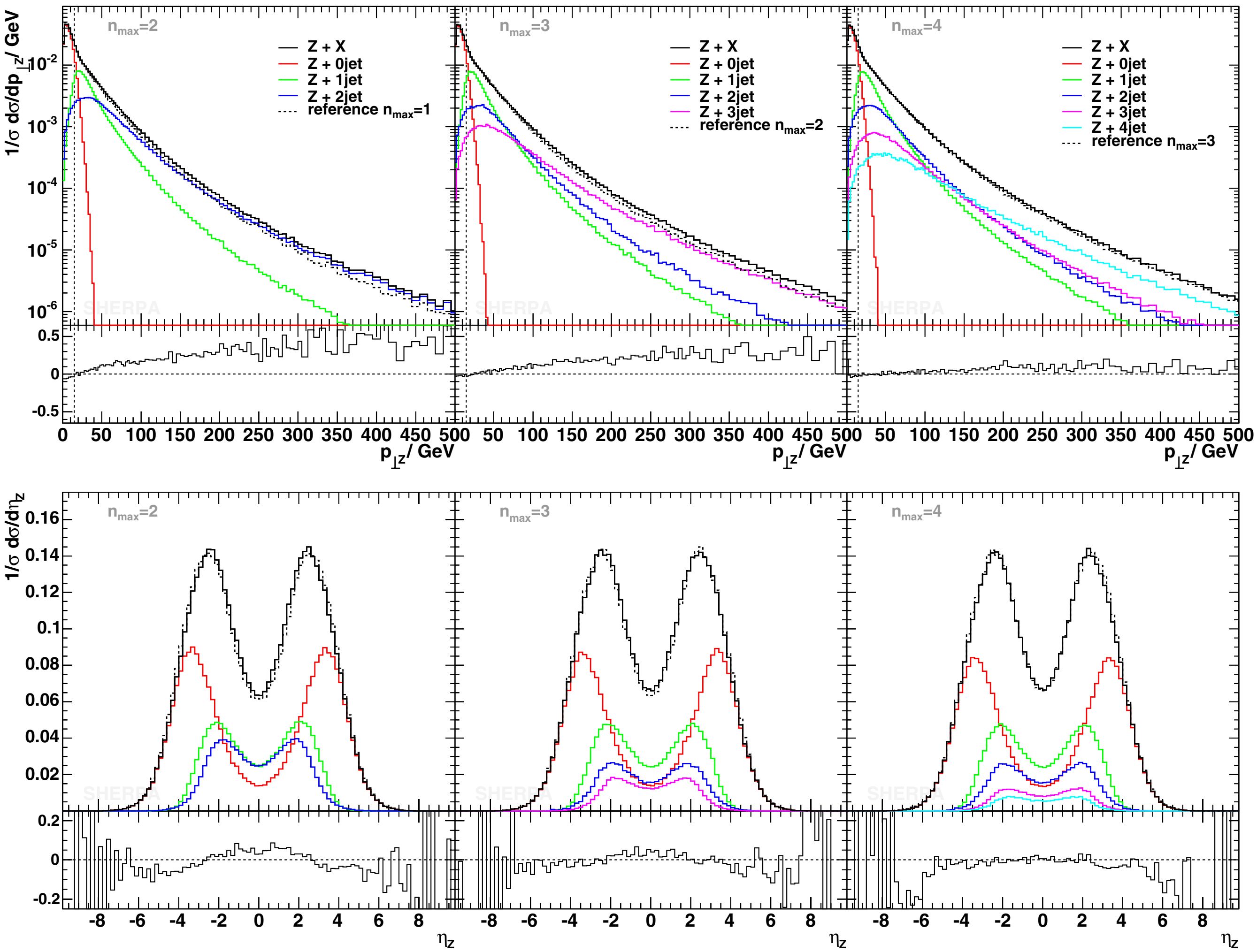

FIG. 3 (color online). $p_\perp(Z)$ (upper row) and $\eta(Z)$ (lower row) for $Q_{\mathrm{cut}} = 15$ GeV and different maximal numbers (2–4, from left to right) of matrix element jets included. The dashed line corresponds to the maximal number of matrix element jets reduced by one. In the lower part of each plot the variations of the result with respect to the corresponding reference curve are presented.

they clearly show how the matrix elements and the parton showers interact in filling the phase space below and above the jet resolution cut. In Fig. 4, differential jet rates using the run II $k_\perp$ clustering algorithm with $R = 1$ are depicted. They signal the relevant Q value of the $k_\perp$ algorithm, where an $(n+1)$-jet event turns into an n-jet event. Again, the results for three different values of Q_{cut} are depicted: from left to right, in the columns $Q_{\mathrm{cut}} = 15$, 30, 100 GeV, as indicated by the thin vertical lines. In each plot, the resulting spectrum is compared to the average of the results for $Q_{\mathrm{cut}} = 15$, 20, 30, 50, 100 GeV. In the three rows, the differential jet rates for the $1 \to 0$, the $2 \to 1$, and for the $3 \to 2$ transitions (from top to bottom) are shown. Starting the discussion with the results for $Q_{\mathrm{cut}} = 30$ GeV, very good agreement with the reference curves can be observed. While the $3 \to 2$ transition is very smooth around the cut, the results for $1 \to 0$ and $2 \to 1$ exhibit small dips at the cut scale. Since the kinematics of the matrix elements is altered when the parton shower is attached, mismatches of the parton configurations close to the cut occur, leading to the dips. Similar structures can be observed for the case of $Q_{\mathrm{cut}} = 100$ GeV. However, more obvious here is that the parton shower fails to fill the phase space for hard emissions up to this very large cut. For $Q_{\mathrm{cut}} = 15$ GeV no visible dips at the cut scale are observed. Instead, this sample seems to slightly overestimate the contributions from higher order matrix elements w.r.t the reference. A small kink at Q_{cut} can be observed for the $1 \to 0$ and $2 \to 1$ transitions.

In Fig. 5 the $p_\perp$ spectrum of the jet in exclusive $Z + 1$ jet production is shown for three choices of the jet resolution scale, $Q_{\mathrm{cut}} = 15$, 50, 100 GeV, indicated by the thin vertical line. The results are contrasted with a reference

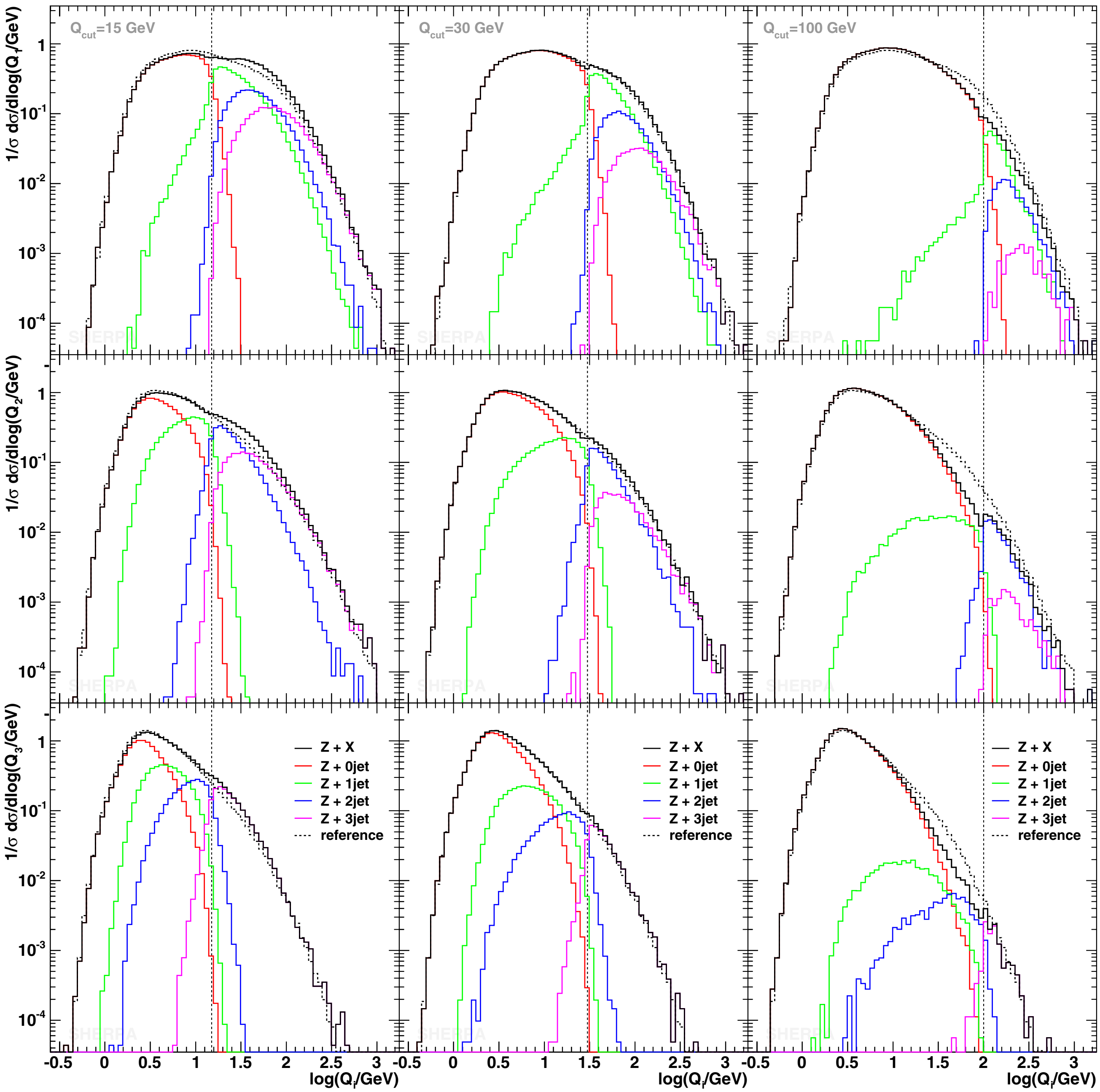

FIG. 4 (color online). Differential jet rates for the $1 \rightarrow 0$, $2 \rightarrow 1$, and $3 \rightarrow 2$ transitions (top to bottom), for $Q_{\mathrm{cut}} = 15$ GeV, 30 GeV, and 100 GeV (from left to right). The dashed reference curve in each plot is obtained after averaging the corresponding results for $Q_{\mathrm{cut}} = 15, 20, 30, 50, 100$ GeV.

curve, again the average of results for $Q_{\mathrm{cut}} = 15, 20, 30, 50, 100$ GeV. The jet has been defined using the run II $k_\perp$ algorithm with a minimal jet $p_\perp$ of 20 GeV and $R = 0.4$. The smallest value of Q_{cut} presented here, namely, 15 GeV, is smaller than the actual jet cut used in the analysis. Accordingly, matrix elements with more than one extra leg have a nonvanishing influence on the jet-$p_\perp$ distribution. This changes as soon as Q_{cut} becomes larger than 20 GeV. For $Q_{\mathrm{cut}} = 50$ GeV and even more for $Q_{\mathrm{cut}} = 100$ GeV the contributions from matrix elements with $n > 1$ are almost negligible. There, only a small dip in the $p_\perp$ distribution around the resolution scale can be observed. As has been seen in the transverse momentum distribution of the lepton pair, cf. Fig. 1, for $Q_{\mathrm{cut}} = 100$ GeV, the shower is not able to fill the full phase space below the cut properly. However, the overall agreement

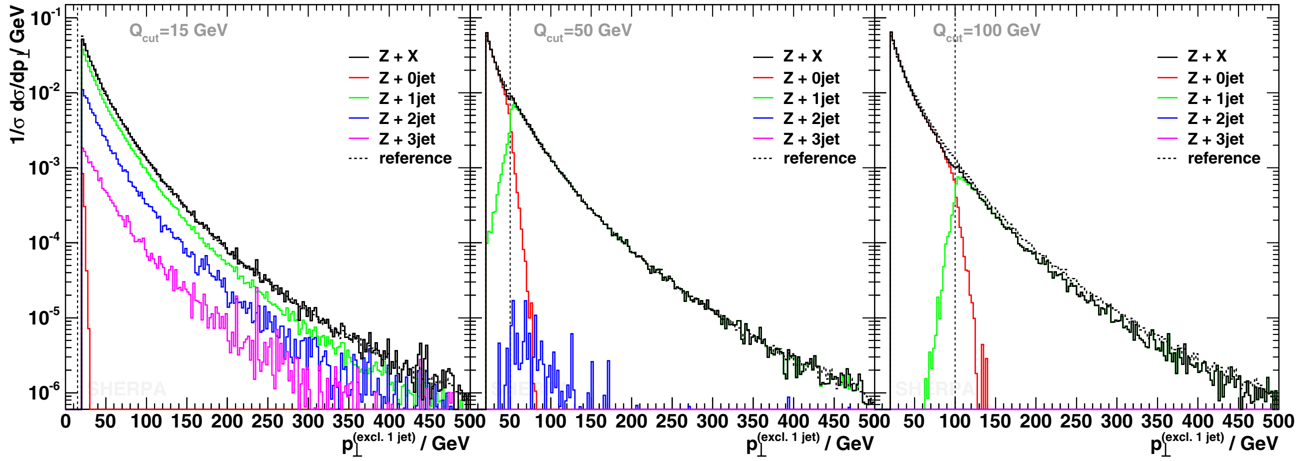

FIG. 5 (color online). $p_\perp$ of the jet in exclusive $Z + 1$ jet production. For the jet definition, the run II $k_\perp$ algorithm with $R = 0.4$ and $p_\perp^{\mathrm{jet}} > 20$ GeV is used. From left to right, results for $Q_{\mathrm{cut}} = 15, 50, 100$ GeV are contrasted with a reference: the average of the results for $Q_{\mathrm{cut}} = 15, 20, 30, 50, 100$ GeV. The thin horizontal line indicates the jet resolution scale used.

of the three results is satisfactory, keeping in mind the large parameter range used for Q_{cut}.

It can be concluded that the cancellation of the Q_{cut} dependence within the SHERPA approach is satisfactory. On top of that, the residual dependence of the results on the parameter Q_{cut} may be used for tuning terms beyond leading logarithmic order to obtain optimal agreement between the Monte Carlo prediction and data.

To highlight the effect of taking into account different maximal numbers of final state partons through matrix elements, a two-jet correlation is exhibited in Fig. 6. There, the relative transverse angle $\Delta\phi$ between the two hardest jets in inclusive $Z + 2$ jet production is displayed; from left to right, $n_{\max}$ has been set to $n_{\max} = 2, 3, 4$. Each result is contrasted with a reference that has been obtained with $n_{\max}^{\mathrm{ref}} = n_{\max} - 1$. From the very left plot it is clear that the one-jet matrix element is incapable of correctly describing the $\Delta\phi$ distribution since the parton shower does not treat interferences properly. On the other hand, as soon as $n_{\max} \geq 2$, the two-jet correlations are consistently described and changes due to the inclusion of higher order matrix elements are rather modest.

C. Variation of renormalization and factorization scales

The algorithm as implemented in SHERPA determines the renormalization and factorization scales used in a specific calculation. Of course, there is some intrinsic freedom in

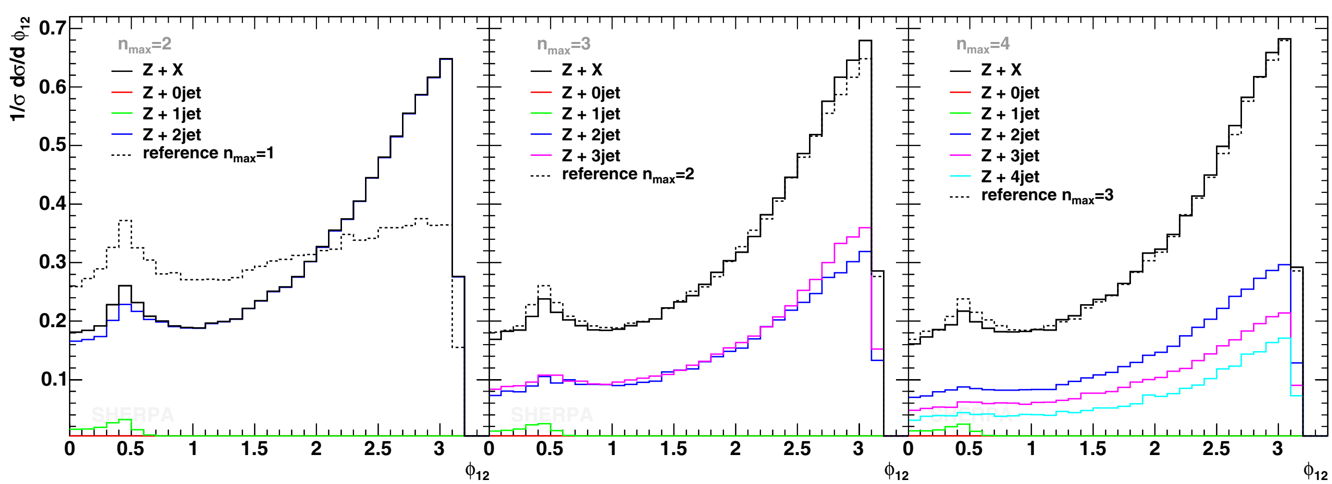

FIG. 6 (color online). $\Delta\phi_{12}$ for $Q_{\mathrm{cut}} = 15$ GeV and different maximal numbers of matrix element jets included. The dashed line corresponds to the reference result obtained with $n_{\max}^{\mathrm{ref}} = n_{\max} - 1$.

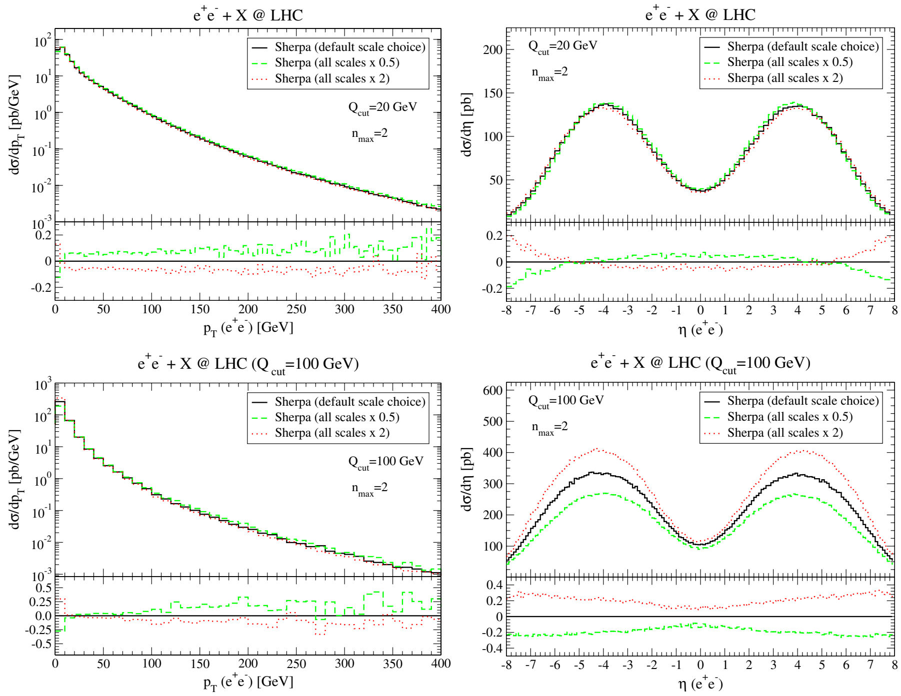

FIG. 7 (color online). The transverse momentum (left) and pseudorapidity (right) distribution of the boson in inclusive Z/γ^* production at the LHC and their dependence on different choices for the factorization and renormalization scales. Results have been obtained using $Q_{\rm cut} = 20$ GeV (upper part) and $Q_{\rm cut} = 100$ GeV (lower part) with $n_{\rm max} = 2$, respectively. The black solid lines indicate the default hadron-level results of SHERPA. To obtain the green dashed (red dotted) lines, all scales appearing in the coupling constants and the PDFs in both the matrix elements and the parton showers are multiplied by a factor of 0.5 (2). In the lower part of each plot the variations of the results with respect to the default scale choice are presented.

defining the scales used for the evaluation of the PDF or the strong coupling constant. In particular, the scales used can be multiplied by constant factors, as long as this alteration is applied both in the matrix element evaluation and reweighting and in the parton shower. This restriction is due to the construction of how the leading logarithmic dependence on $Q_{\rm cut}$ is eliminated. The dependence of the SHERPA results with respect to such scale variations is studied in Figs. 7 and 8. Results obtained with the default scale choices are confronted with results obtained when all scales appearing in the coupling constants and PDFs are multiplied by common factors of 0.5 and 2.

In Fig. 7 the transverse momentum and pseudorapidity distribution of the Z/γ^* boson are depicted for two different values of $Q_{\rm cut}$, namely, $Q_{\rm cut} = 20$ GeV and $Q_{\rm cut} = 100$ GeV. For the case of the $p_\perp$ distributions, except for the very first bins the spectra obtained with a factor of 0.5 (2) are always above (below) the default results. The differences are rather constant and of the order of 10%–15% for $Q_{\rm cut} = 20$ GeV and 20%–25% for $Q_{\rm cut} = 100$ GeV. As has been seen before, cf. Figs. 1 and 3, for transverse momenta above the cut scale, the distribution is predominantly described by higher order matrix elements, whose scale dependence at leading order is known to be reversed with respect to the lowest order process [19]. This lowest order process, however, dominates the region of low boson momenta. There the $2 \to 2$ cross section exhibits a strong decline when the scales become smaller. This effect potentially leads to the reversal of the discrepancies in the soft region. It is interesting to note that for the case of $Q_{\rm cut} = 100$ GeV the parton shower is able to tame the scale variations of the result between $10\ {\rm GeV} < p_\perp < 100$ GeV. For the case of the pseudorapidity distribution, the differences for the two values of $Q_{\rm cut}$ are more pronounced. From Figs. 2 and 3 one can read off the composition of the different samples. For $Q_{\rm cut} = 20$ GeV only the region of large values of $|\eta|$ is described by the parton shower attached to the $2 \to 2$ matrix element. For $|\eta| > 5$ the spectrum where all scales have been multiplied by a factor of 2 is enhanced up to 20%. A factor of 0.5, on the other hand, depopulates this phase-space region by up to 20%. In the intermediate range of pseudorapidity the deviations of the two spectra from the default scale choice are well below 10%. For the sample with $Q_{\rm cut} = 100$ GeV, almost the whole distribution is described by the $2 \to 2$ matrix element plus parton shower only. Accordingly, the deviations found before in the region of large values of $|\eta|$ now extend over the whole range of the distribution. The scale variations are of the order of 20%–25% and are damped only in the very central region of pseudorapidity, the region of phase space where higher order matrix elements play a role.

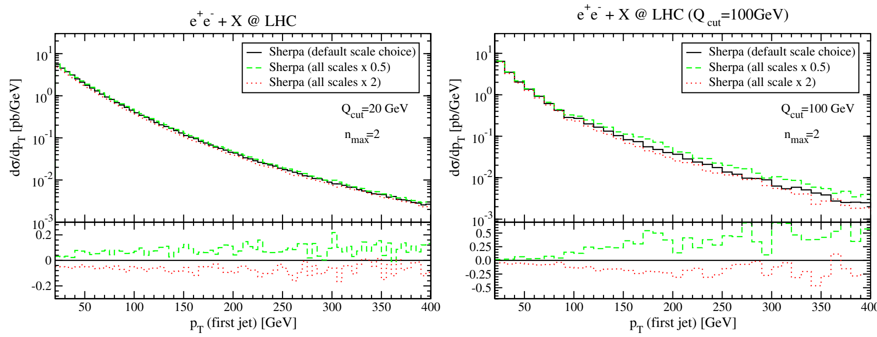

FIG. 8 (color online). The $p_\perp$ spectrum of the hardest jet in inclusive Z/γ^* production at the LHC and its dependence on different choices for the factorization and renormalization scale. Results have been obtained using $Q_{\rm cut} = 20$ GeV (left panel) and $Q_{\rm cut} = 100$ GeV (right panel) and $n_{\max} = 2$, respectively. Jets are defined through the run II $k_\perp$ algorithm with $R = 0.4$ and $p_\perp^{\rm jet} > 20$ GeV. The black solid lines correspond to the default hadron-level results of SHERPA. To obtain the green dashed (red dotted) lines, all scales appearing in the coupling constants and the PDFs in both the matrix elements and the parton showers are multiplied by a factor of 0.5 (2). In the lower part of the plots the variations of the results with respect to the default scale choice are presented.

In Fig. 8 the transverse momentum distribution of the hardest jet in inclusive Z/γ^* production is depicted. For $Q_{\rm cut} = 20$ GeV the result has no significant contribution from the leading order $2 \to 2$ process. Therefore, the two results obtained after scale manipulation do not cross each other. Over the whole range of jet transverse momentum the deviations of the two curves from the default result are very moderate. For $Q_{\rm cut} = 100$ GeV the deviations for large values of jet transverse momentum are enhanced. This may be due to the larger value of the factorization scale used in the here dominating one-jet process. Multiplying this scale, $\mu_{\rm fac} = Q_{\rm cut}$, by factors of 0.5 or 2 results in a broader band of scales tested. Contrary to that, the region described by the parton shower, namely, $p_\perp < 100$ GeV, shows a rather mild dependence upon the scale choice, similar to what is observed in Fig. 7 for moderate boson transverse momenta.

It can be concluded that the predictions of SHERPA show rather mild variations over a wide range of the phase space when multiplying all scales appearing in the coupling constants and PDFs by common factors of 0.5 and 2. The largest deviations from the default choice of scales are observed in those phase-space regions that are predominantly covered by the $2 \to 2$ matrix element with the parton shower attached.

III. SHERPA VS NLO RESULTS

Having investigated the self-consistency of the merging procedure as implemented in SHERPA, its parton level results are compared with those from MCFM, V. 4.0, [18,19]. For the class of processes studied here, MCFM is capable of calculating total and fully differential cross sections at next-to-leading order in the strong coupling constant for $(Z/\gamma^* \to l^+ l^-) + 0, 1, 2$ and $(W^\pm \to l\nu_l) + 0, 1, 2$ partons. For all calculations with MCFM, the cteq6l [56] PDF has been used, and $\alpha_S(m_Z) = 0.118$ in accordance with the value of the PDF evolution. The renormal-

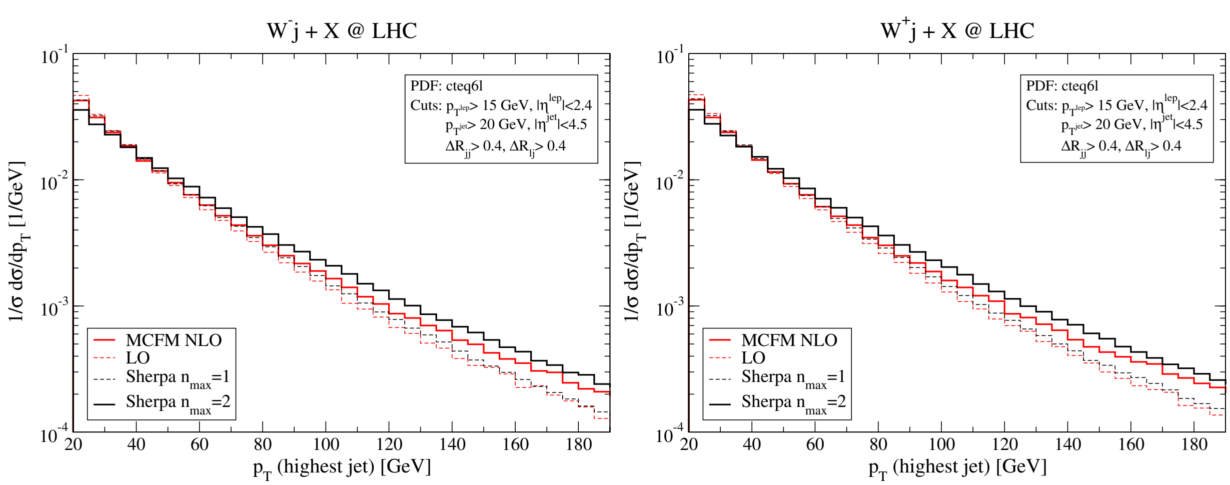

FIG. 9 (color online). The p_T distribution of the hardest jet for inclusive W^- (left panel) and W^+ (right panel) plus one-jet events at the LHC.

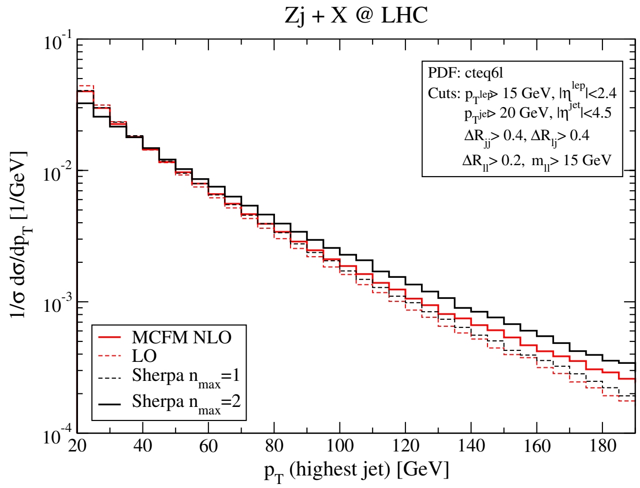

FIG. 10 (color online). The p_T distribution of the hardest jet for inclusive Z/γ^* plus one-jet events at the LHC.

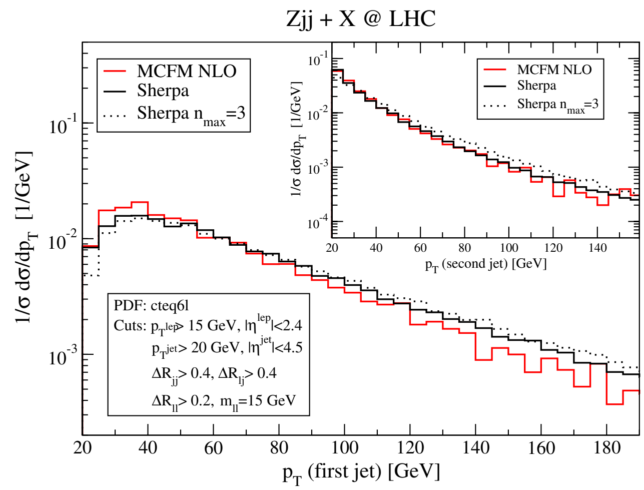

FIG. 12 (color online). The p_T distribution of the two hardest jets in inclusive Z/γ^* plus two-jet production at the LHC.

ization and factorization scales have been chosen to be identical with the bosons' mass, i.e. $\mu_R = \mu_F = \mathrm{m_Z}$ or $\mu_R = \mu_F = \mathrm{m_W}$, respectively. Phase-space cuts are listed in Appendix A. In contrast to a previous publication [36], this time only inclusive quantities are compared. For the next-to-leading order calculation this translates into an unconstrained phase space for the real higher order correction. Thus, the higher order corrections may give rise to an additional jet. The SHERPA results were obtained after the parton shower evolution. For the sake of a better comparison, all curves have been normalized to one, eliminating the enhancement of the cross section due to the NLO corrections.

First of all, in Figs. 9 and 10 the $p_\perp$ spectra of the hardest jet in inclusive $W^+ + 1$ jet, $W^- + 1$ jet, and $Z/\gamma^* + 1$ jet production are exhibited. For all cases, results at leading and at next-to-leading order were contrasted with results from SHERPA for $n_{\max} = 1$ or $n_{\max} = 2$ and $Q_{\mathrm{cut}} = 20$ GeV. In all plots the high-$p_\perp$ tail is significantly enhanced when going from LO to NLO. The SHERPA samples with $n_{\max} = 2$ show the same behavior but tend to pronounce the high-$p_\perp$ region even more. This is in striking contrast to the $n_{\max} = 1$ samples. They are incapable of recovering the shape of the distribution at NLO, and tend to look like the LO result. This is not surprising. The NLO calculation takes into account tree-level matrix elements with two final state partons as the real contribution to the NLO result. Because of the large phase space available at the LHC, this real contribution tends to produce an extra jet that alters the kinematics of the first jet. Obviously this significant change in the kinematics cannot be appropriately recovered by the parton shower. The $n_{\max} = 2$ SHERPA samples also include the parton shower, resulting in increased parton emission thus enhancing the high-$p_\perp$ tail even more. It would for sure be instructive to check this behavior with a resummed NLO computation for these processes.

In Figs. 11 and 12 the $p_\perp$ spectra of the two hardest jets in inclusive $W^+ + 2$ jet, $W^- + 2$ jet, and $Z/\gamma^* + 2$ jet production are displayed. This time, next-to-leading order

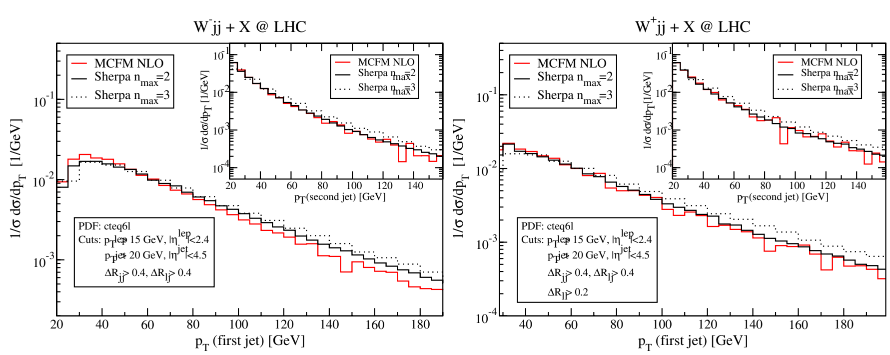

FIG. 11 (color online). The p_T distribution of the two hardest jets in inclusive W^- (left panel) and W^+ (right panel) plus two-jet production at the LHC.

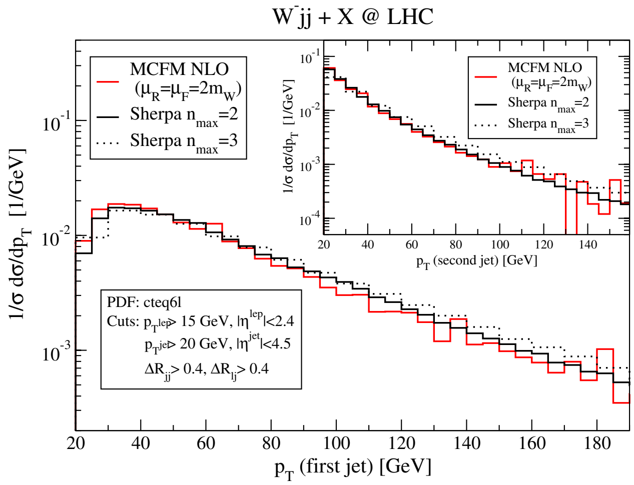

FIG. 13 (color online). The p_T distribution of the first and second hardest jets in inclusive W^- plus two-jet production at the LHC. For the NLO calculation the renormalization and factorization scales have been chosen to $\mu_R = \mu_F = 2\mathrm{m_W}$.

results from MCFM are compared with the corresponding SHERPA samples with $n_{\max} = 2$ and $n_{\max} = 3$ and $Q_{\mathrm{cut}} = 20$ GeV. It has been shown in [19] that the shapes of the distributions when going from LO to NLO are quite stable. The slopes of the next-to-leading order and the SHERPA results are in good agreement. However, the SHERPA results have the tendency to produce the first jet slightly harder than the NLO prediction. This is even more pronounced for the sample with $n_{\max} = 3$ where the maximal number of matrix element legs used within SHERPA is equal to the one used in the NLO computation for the real corrections. In Fig. 13 the $p_\perp$ spectra of the two hardest jets in inclusive $W^- + 2$ jet production are displayed once more. This time, however, the renormalization and factorization scales in the NLO calculations have been chosen as $\mu_R = \mu_F = 2\mathrm{m_W}$. For this choice of the scales the agreement of MCFM and SHERPA is even better. This highlights the effect of scale variations, a good way to estimate residual uncertainties due to higher order corrections, and shows that the results of SHERPA are well within theoretical uncertainties.[1]

IV. SHERPA VS MC@NLO AND PYTHIA

In this section, hadron-level results of SHERPA will be compared with those of two other event generators, namely, MC@NLO [41–43] and PYTHIA [37,38]. The former program incorporates a consistent matching of a full-fledged next-to-leading order calculation with the parton shower provided by HERWIG [39,40]. It thus employs an angular-ordered shower, taking full account of coherence effects. In contrast, PYTHIA uses tree-level matrix elements, in this case for $q\bar{q} \to e^+e^-$, and it employs a virtuality-ordered parton shower to model further emissions. In this framework, coherence effects are approximated through an explicit veto on rising opening angles in the splitting. Hence, the parton shower implementations of PYTHIA and SHERPA are quite similar. However, in order to account for, in PYTHIA, jets with a $p_\perp$ larger than the "natural" starting scale of the parton shower equal to the invariant mass of the lepton pair, the starting scale has been increased to the center-of-mass energy of the proton-proton system, i.e. to 14 TeV. This choice is supplemented with a matrix element correction procedure implemented through reweighting meant to reproduce the exact matrix element for the emission of an additional jet. The precise setups for both codes can be found in Appendix B.

First of all, the results of the three programs for some rather inclusive quantities are compared. The transverse momentum and pseudorapidity distributions of the produced bosons are presented in Figs. 14 and 15. The SHERPA predictions depicted have been obtained with $n_{\max} = 1$ and $Q_{\mathrm{cut}} = 20$ GeV, in order to match the approaches of the other codes. In order to compare the different samples, they all have been subject to a cut on the boson invariant mass of the form

$$m_V - 30 \cdot \Gamma_V \leq m_V^* \leq m_V + 30 \cdot \Gamma_V, \tag{1}$$

where no additional phase-space cuts have been applied. All distributions have been normalized to their respective cross section.

The results for both processes look very similar. The boson transverse momentum distributions of MC@NLO and SHERPA agree fairly well. In the case of Z/γ^* production they match nearly perfectly for values of $p_\perp > 100$ GeV. In the intermediate range of 10 GeV $< p_\perp <$ 100 GeV SHERPA apparently is below MC@NLO. This discrepancy may have its origin in the different shower approaches used within the two programs. This statement is also hinted at by the fact that the PYTHIA result follows the SHERPA distribution for $p_\perp < 35$ GeV. For larger values of $p_\perp$, however, the PYTHIA distribution is far below MC@NLO and SHERPA predicting much less bosons with large transverse momentum. For the case of W^+ production the MC@NLO and SHERPA predictions cross at $p_\perp \approx 60$ GeV. SHERPA produces slightly less events with smaller boson $p_\perp$ and tends to pronounce the high $p_\perp$ region a bit. Again PYTHIA produces fewer bosons with intermediate and large boson transverse momenta. Looking at the pseudorapidity distributions, it can be recognized that MC@NLO and SHERPA both tend to produce the bosons much more central than PYTHIA. The region of $|\eta| < 4$ is especially filled significantly with respect to PYTHIA, which, in contrast, features a much broader shape. This effect is of course directly correlated to the larger amount of hard QCD radiation the other two programs produce, since this enhanced

[1] It should be noted that the effect of this scale variation on the total cross section is merely of the order of 1%, although the shape of the distribution in the high-$p_\perp$ tail changes considerably.

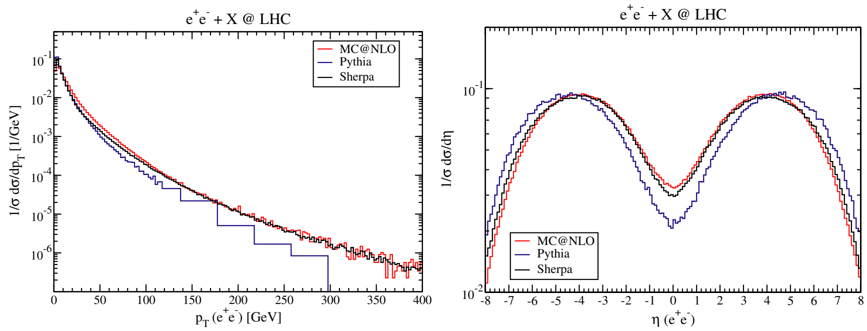

FIG. 14 (color online). The $p_\perp$ (left) and η (right) distribution of the lepton pair in inclusive production of a Z/γ^* boson decaying into e^+e^- at the LHC. The results of the generators MC@NLO, PYTHIA, and SHERPA are compared.

QCD radiation allows for larger boson recoils. Moreover, from Fig. 3 it can be anticipated how the SHERPA results change under the inclusion of matrix elements with extra QCD legs: the boson transverse momentum distribution develops a more pronounced large-$p_\perp$ tail and the very central region of η is filled even more, thus reducing the amount of events with large values of $|\eta|$. So while the $p_\perp$ spectra would be slightly harder than those of MC@NLO the η distributions would fit even better than they do for the case of including $V + 0$ and $V + 1$ parton matrix elements only.

For the comparison of jet observables, only the case of Z/γ^* production is studied. The qualitative statements implied by it, however, will hold true as well in the case of W production. To judge the abilities of the three programs to produce extra hard QCD radiation associated with the electroweak gauge bosons, the transverse momentum distribution of the first (second) hardest jet in events with at least one (two) extra jet(s) is depicted in Fig. 16. In addition, Fig. 17 presents the transverse momentum spectrum of the third jet in events with at least three extra jets. For this comparison in addition to the cut on the boson transverse mass according to Eq. (1), the jet criteria and phase-space cuts of Appendix A have been applied. For SHERPA the jet resolution parameter has been set to $Q_{\mathrm{cut}} = 20$ GeV. The standard sample for this comparison uses again only matrix elements with up to one additional parton. To test the predictions of SHERPA samples with $n_{\max} = 2(3)$ have been considered as well; the corresponding results are shown as dashed (dotted) lines in the plots. Since it is actually the production rate that is important here, this time the curves have not been normalized. Instead the corresponding differential cross sections are presented.

For the hardest jet the predictions of MC@NLO and SHERPA agree rather well. The total rate of SHERPA is 12% smaller than that predicted by MC@NLO; the distribution, however, has a slightly harder tail. This difference in rate can be traced back to the different inclusive production cross sections. However, for $n_{\max} = 2$, the two total cross sections of $Z + 1$ jet nearly coincide (cf. the dashed black curve in Fig. 16). In terms of shape, SHERPA apparently favors jets with larger transverse momentum. As has been seen in the closely related boson $p_\perp$ distribution in Fig. 14, PYTHIA predicts a much smaller rate (60% w.r.t. the rate predicted by MC@NLO) for the production of extra hard QCD radiation with a softer distribution.

For the second jet the situation changes significantly. Here, even in the case of including only matrix elements with up to one extra parton, the two-jet rate predicted by

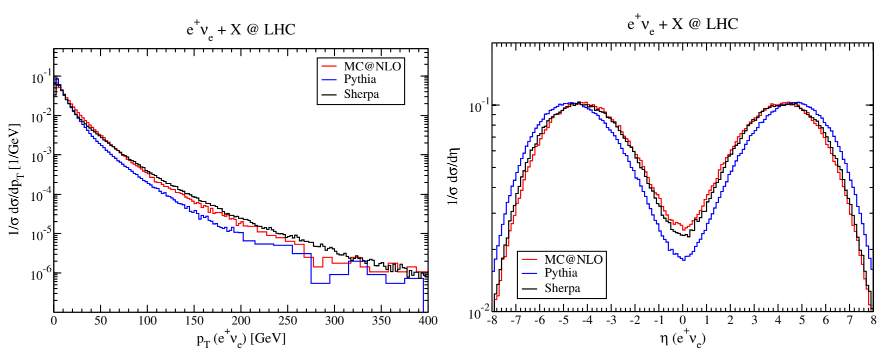

FIG. 15 (color online). The W^+ $p_\perp$ (left) and η (right) distributions in inclusive production at the LHC. The results of the generators MC@NLO, PYTHIA, and SHERPA are compared.

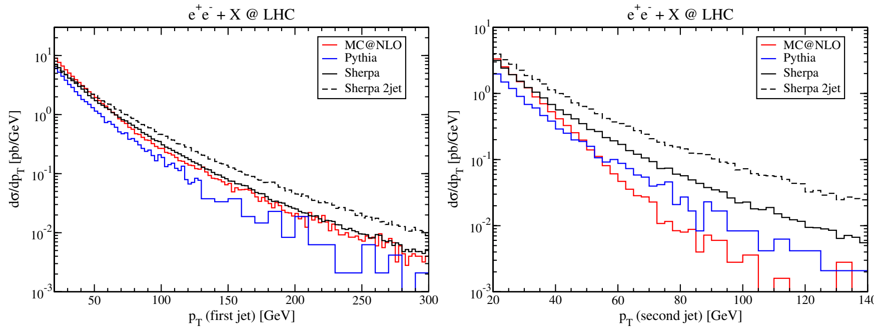

FIG. 16 (color online). The $p_\perp$ distribution of the first (left) and second (right) hardest jet in inclusive Z/γ^* production at the LHC as obtained by MC@NLO, PYTHIA, and SHERPA. The dashed lines correspond to the predictions of SHERPA when matrix elements for up to two additional partons are used.

SHERPA is 17% larger than that of MC@NLO. Including matrix elements with two extra partons the difference becomes nearly 90%. As for the case of the first jet, PYTHIA predicts the radiation of a second jet with a much smaller rate. Similar statements hold true when looking at the third jet but this time the differences are even larger. Note that a reliable prediction of the three-jet rate requires the inclusion of matrix elements with at least three extra partons. While the sample with matrix elements up to one extra parton predicts a three-jet rate of 9.6 pb, the samples with two (three) extra partons predict 16.3(21.1) pb. However, this is not surprising keeping in mind that the LHC provides enough phase space to produce massive bosons in association with a multitude of high energetic jets that are best described by the corresponding matrix elements and that cannot be appropriately described by parton shower emissions.

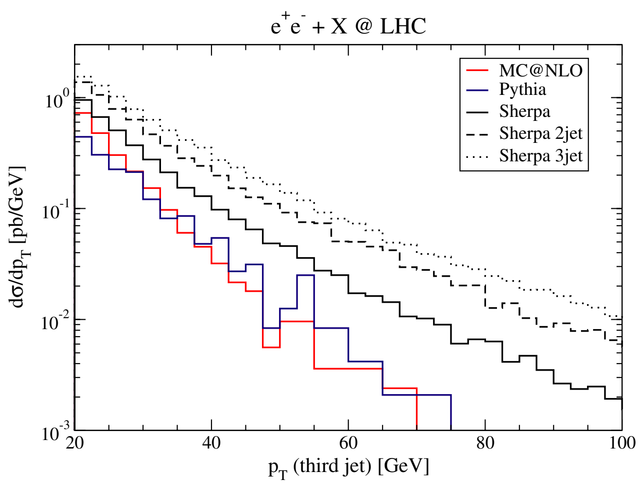

FIG. 17 (color online). The $p_\perp$ distribution of the third hardest jet in inclusive Z/γ^* production at the LHC as obtained by MC@NLO, PYTHIA, and SHERPA. The dashed (dotted) line corresponds to the prediction of SHERPA when matrix elements for up to two (three) additional partons are used.

To summarize, the predictions of MC@NLO and SHERPA agree fairly well for the shape of the boson transverse momentum and pseudorapidity distribution. Here, MC@NLO is of course superior in predicting the rate of inclusive Z/γ^* and W production since it considers the corresponding production process at NLO in the coupling constant. This situation changes when studying the jets that potentially accompany the boson. As soon as more than one extra jet is considered SHERPA predicts significantly larger jet production rates and jet transverse momentum distributions that feature an enhanced population of the high-$p_\perp$ region. Concerning PYTHIA it has to be stated that the shape of the boson transverse momentum and the boson pseudorapidity distribution differ significantly from the two other programs. This is directly related to the smaller amount of hard radiation produced by PYTHIA, clearly observed in the jet $p_\perp$ spectra.

V. SUMMARY

In this publication, the previous validation of the merging procedure of matrix elements and the parton shower, as implemented in SHERPA, has been continued. Again, processes of the type $pp \to V + X$, where $V = W^\pm, Z/\gamma^*$, have been chosen; this time, however, the analysis focused on the case of the CERN LHC rather than on the Fermilab Tevatron. Again, the merging procedure turned out to yield sufficiently stable results over a wide range of internal parameters, rendering it a predictive way of incorporating the full information available in tree-level matrix elements into multipurpose event generators, as anticipated. In addition, when comparing the results obtained through SHERPA with those of a full next-to-leading order calculation, it again turned out that the results of SHERPA reproduce the essential features in the NLO shapes. However, it should be stressed that in SHERPA the total rates are still at leading order accuracy only. Nevertheless, since SHERPA seems to reproduce the NLO shapes of the observables, the

NLO rates can be recovered by simply multiplying with a constant K factor. When comparing the results of SHERPA with those of other event generators, some differences appear. Especially for observables sensitive to the correct treatment of multiparticle final states, these differences have become significant and can be larger than one order of magnitude.

In this study, SHERPA again proved its versatility in simulating high-multiplicity final states at collider experiments. Because of the merging procedure implemented in it, it provides a unique tool for the simulation of final states, where the proper treatment of the event topology is of great importance.

ACKNOWLEDGMENTS

The authors would like to thank T. Gleisberg, S. Höche, and J. Winter for pleasant collaboration on SHERPA and M. L. Mangano and J. Campbell for helpful discussions. Financial support by BMBF, DESY-PT, GSI, and DFG is gratefully acknowledged.

APPENDIX A: INPUT PARAMETERS AND PHASE-SPACE CUTS

For all analyses, the PDF set cteq6l [56] has been used, and α_S has been chosen according to the corresponding value of this PDF, namely, $\alpha_S = 0.118$. For the running of the strong coupling constant, the corresponding two-loop equation has been employed. Jets or initial partons are restricted to the light flavor sector, namely, g, u, d, s, and c. All flavors are taken to be massless.

1. Standard model input parameters

The standard model (SM) parameters are given in the G_μ scheme:

$$\begin{aligned} &m_W = 80.419\ \text{GeV}, \qquad \Gamma_W = 2.06\ \text{GeV},\\ &m_Z = 91.188\ \text{GeV}, \qquad \Gamma_Z = 2.49\ \text{GeV},\\ &G_\mu = 1.16639 \times 10^{-5}\ \text{GeV}^{-2},\\ &\sin^2\theta_W = 1 - m_W^2/m_Z^2, \qquad \alpha_s = 0.118. \end{aligned} \tag{A1}$$

The electromagnetic coupling is derived from the Fermi constant G_μ according to

$$\alpha_{\text{em}} = \frac{\sqrt{2} G_\mu M_W^2 \sin^2\theta_W}{\pi}. \tag{A2}$$

The constant widths of the electroweak gauge bosons are introduced through the fixed-width scheme. Cabibbo-Kobayashi-Maskawa mixing of the quark generations is neglected.

2. Cuts and jet criteria

For all jet analysis, the run II $k_\perp$ clustering algorithm defined in [57] has been used. The additional parameter of this jet algorithm is a pseudocone size R, whose value has been chosen as $R = 0.4$. In addition, jets have to fulfill the following cuts on transverse momentum and pseudorapidity,

$$p_T^{\text{jet}} > 20\ \text{GeV}, \qquad |\eta^{\text{jet}}| < 4.5. \tag{A3}$$

For charged leptons the cuts applied are

$$p_T^{\text{lepton}} > 15\ \text{GeV}, \qquad |\eta^{\text{lepton}}| < 2.4, \qquad m_{ll} > 15\ \text{GeV}. \tag{A4}$$

No cut on missing transverse momentum has been applied.

The final selection criteria correspond to the separation of the leptons amongst each other and with respect to the jets,

$$\Delta R_{lj} > 0.4, \qquad \Delta R_{ll} > 0.2. \tag{A5}$$

APPENDIX B: SETUPS FOR MC@NLO AND PYTHIA

(i) *The* MC@NLO *setup*: The program version used is MC@NLO 2.31. The process number corresponding to $pp \to Z/\gamma^* \to e^+e^- + X$ production is IPROC $= -11351$; for $pp \to W^+ \to e^+\nu_e + X$ this equals IPROC $= -11461$. In both cases, consequently, the underlying event has been switched off. The lepton pair in Z/γ^* production has been generated in a mass window of

$$m_Z - 30\Gamma_Z \le m_{ee} \le m_Z + 30\Gamma_Z; \tag{B1}$$

in the case of W^+ production the lepton-neutrino pair fulfills

$$m_W - 30\Gamma_W \le m_{e\nu_e} \le m_W + 30\Gamma_W. \tag{B2}$$

The PDF set used is cteq6l. All other physics parameters that specify a run for MC@NLO have been left unchanged with respect to their default values.

(ii) *The* PYTHIA *setup*: The PYTHIA version used is 6.214. The process $pp \to Z/\gamma^* + X$ is selected via the parameter MSUB(1) $= 1$. The decay mode $Z/\gamma^* \to e^+e^-$ is picked by the settings MDME(182, 1) $= 1$ and MDME(170, 1) $= 1$; all other decay channels have been disabled. The process $pp \to W^+ + X$ is turned on via MSUB(2) $= 1$. The decay mode $W^+ \to e^+\nu_e$ is chosen by MDME(206, 1) $= 1$. It has proven to be convenient to increase the standard value of the shower starting scale in PYTHIA to $\sqrt{s} = 14$ TeV in order to produce a reasonable amount of high energetic QCD radiation. The parameter responsible for controlling the shower start scales is MSTP(68). For the above choice it has to be set to MSTP(68) $= 2$. All other parameters specific for PYTHIA have been left unaltered, except that PYTHIA's underlying event has been switched off.

[1] G. Altarelli, R. K. Ellis, and G. Martinelli, Nucl. Phys. **B157**, 461 (1979).
[2] J. Kubar-Andre and F. E. Paige, Phys. Rev. D **19**, 221 (1979).
[3] K. Harada, T. Kaneko, and N. Sakai, Nucl. Phys. **B155**, 169 (1979); **B165**, 545(E) (1980).
[4] J. Abad and B. Humpert, Phys. Lett. B **80**, 286 (1979).
[5] B. Humpert and W. L. Van Neerven, Phys. Lett. B **85**, 293 (1979).
[6] R. Hamberg, W. L. van Neerven, and T. Matsuura, Nucl. Phys. **B359**, 343 (1991); **B644**, 403(E) (2002).
[7] R. V. Harlander and W. B. Kilgore, Phys. Rev. Lett. **88**, 201801 (2002).
[8] C. Anastasiou, L. J. Dixon, K. Melnikov, and F. Petriello, Phys. Rev. D **69**, 094008 (2004).
[9] C. Balazs and C. P. Yuan, Phys. Rev. D **56**, 5558 (1997).
[10] F. A. Berends, H. Kuijf, B. Tausk, and W. T. Giele, Nucl. Phys. **B357**, 32 (1991).
[11] A. Pukhov *et al.*, hep-ph/9908288.
[12] T. Ishikawa, T. Kaneko, K. Kato, S. Kawabata, Y. Shimizu, and H. Tanaka (MINAMI-TATEYA Group Collaboration), KEK Report No. KEK-92-19.
[13] K. Sato *et al.*, in *Proceedings of the VII International Workshop on Advanced Computing and Analysis Techniques in Physics Research (ACAT 2000)*, P. C. Bhat and M. Kasemann, AIP Conf. Proc. No. 583 (AIP, New York, 2001), p. 214.
[14] T. Stelzer and W. F. Long, Comput. Phys. Commun. **81**, 357 (1994).
[15] F. Maltoni and T. Stelzer, J. High Energy Phys. 02 (2003) 027.
[16] M. L. Mangano, M. Moretti, F. Piccinini, R. Pittau, and A. D. Polosa, J. High Energy Phys. 07 (2003) 001.
[17] F. Krauss, R. Kuhn, and G. Soff, J. High Energy Phys. 02 (2002) 044.
[18] J. Campbell and R. K. Ellis, Phys. Rev. D **65**, 113007 (2002).
[19] J. Campbell, R. K. Ellis, and D. L. Rainwater, Phys. Rev. D **68**, 094021 (2003).
[20] V. A. Khoze, A. D. Martin, R. Orava, and M. G. Ryskin, Eur. Phys. J. C **19**, 313 (2001).
[21] M. Dittmar, F. Pauss, and D. Zurcher, Phys. Rev. D **56**, 7284 (1997).
[22] A. D. Martin, R. G. Roberts, W. J. Stirling, and R. S. Thorne, Eur. Phys. J. C **14**, 133 (2000).
[23] W. T. Giele and S. A. Keller, hep-ph/0104053.
[24] ATLAS Collaboration, "*Detector and Physics Performance Technical Design Report*," CERN Report No. CERN/LHCC/99-15, Vol. 2.
[25] S. Haywood *et al.*, hep-ph/0003275.
[26] S. Abachi *et al.* (D0 Collaboration), Phys. Rev. Lett. **75**, 1456 (1995).
[27] T. Affolder *et al.* (CDF Collaboration), Phys. Rev. D **64**, 052001 (2001).
[28] V. M. Abazov *et al.* (D0 Collaboration), Phys. Rev. D **66**, 012001 (2002).
[29] W. Ashmanskas *et al.* (Tevatron Electroweak Working Group, CDF Collaboration, and D0 Collaboration) Phys. Rev. D **70**, 092008 (2004).
[30] C. Albajar *et al.* (UA1 Collaboration), Phys. Lett. B **253**, 503 (1991).
[31] J. Alitti *et al.* (UA2 Collaboration), Phys. Lett. B **276**, 365 (1992).
[32] F. Abe *et al.* (CDF Collaboration), Phys. Rev. D **52**, 2624 (1995).
[33] B. Abbott *et al.* (D0 Collaboration), Phys. Rev. D **61**, 072001 (2000).
[34] T. Affolder *et al.* (CDF Collaboration), Phys. Rev. Lett. **85**, 3347 (2000).
[35] V. M. Abazov *et al.* (D0 Collaboration), Phys. Rev. D **66**, 032008 (2002).
[36] F. Krauss, A. Schälicke, S. Schumann, and G. Soff, Phys. Rev. D **70**, 114009 (2004).
[37] T. Sjöstrand, Comput. Phys. Commun. **82**, 74 (1994).
[38] T. Sjöstrand, L. Lönnblad, and S. Mrenna, hep-ph/0108264.
[39] G. Corcella *et al.*, J. High Energy Phys. 01 (2001) 010.
[40] G. Corcella *et al.*, hep-ph/0210213.
[41] S. Frixione and B. R. Webber, J. High Energy Phys. 06 (2002) 029.
[42] S. Frixione, P. Nason, and B. R. Webber, J. High Energy Phys. 08 (2003) 007.
[43] S. Frixione and B. R. Webber, hep-ph/0402116.
[44] T. Gleisberg, S. Höche, F. Krauss, A. Schälicke, S. Schumann, and J. C. Winter, J. High Energy Phys. 02 (2004) 056.
[45] M. H. Seymour, Comput. Phys. Commun. **90**, 95 (1995).
[46] G. Miu and T. Sjöstrand, Phys. Lett. B **449**, 313 (1999).
[47] G. Corcella and M. H. Seymour, Nucl. Phys. **B565**, 227 (2000).
[48] S. Catani, Y. L. Dokshitzer, M. Olsson, G. Turnock, and B. R. Webber, Phys. Lett. B **269**, 432 (1991).
[49] S. Catani, Y. L. Dokshitzer, and B. R. Webber, Phys. Lett. B **285**, 291 (1992).
[50] S. Catani, Y. L. Dokshitzer, M. H. Seymour, and B. R. Webber, Nucl. Phys. **B406**, 187 (1993).
[51] S. Catani, F. Krauss, R. Kuhn, and B. R. Webber,J. High Energy Phys. 11 (2001) 063.
[52] F. Krauss, J. High Energy Phys. 08 (2002) 015.
[53] L. Lönnblad, J. High Energy Phys. 05 (2002) 046.
[54] S. Mrenna and P. Richardson, J. High Energy Phys. 05 (2004) 040.
[55] M. L. Mangano, M. Moretti, and R. Pittau, Nucl. Phys. **B632**, 343 (2002).
[56] J. Pumplin, D. R. Stump, J. Huston, H. L. Lai, P. Nadolsky, and W. K. Tung, J. High Energy Phys. 07 (2002) 012.
[57] G. C. Blazey *et al.*, hep-ex/0005012.